Fatigue Fract. Engng Mater. Struct. Vol. 15, No. 10, pp. 1009–1024, 1992
Printed in Great Britain.

8756-758X/92 $5.00 + 0.00

FRACTURE BEHAVIOUR OF AXISYMMETRIC BARS UNDER HIGH TRIAXIAL STRESS AND LARGE STRAIN CYCLIC LOADING

M. L. DU[1], G. C. LI[1], Y. Z. ZHANG[2] and W. D. FANG[2]

[1]Institute of Mechanics, Academia Sinica, Beijing 100080 and [2]Department of Material Science and Engineering, Huazhong University of Science and Technology, Wuhan 430074, People's Republic of China

(Received in final form 30 April 1992)

Abstract—Axisymmetric notched bars with notch roots of large and small radii were tested under large strain cyclic loading. The main attention is focused on the fracture behaviour of steels having cycles to failure within the range 1–100. Our study shows that a gradual transition from a static ductile nature to one of fatigue cleavage can be observed and characterized by the Coffin–Manson formula in a generalized form. Both the triaxial tensile stress within the central region of specimens and static damage caused by the first increasing load have effects on the final failure event. A generalized cyclic strain range parameter $\Delta\epsilon$ is proposed as a measure of the numerous factors affecting behaviour. Fractographs are presented to illustrate the behaviour reported in the paper.

NOMENCLATURE

$\Delta\epsilon$ = generalized cyclic strain range
$\Delta\bar{\epsilon}$ = the average plastic strain range during the whole life
ϵ_d = radial strain at the minimum section
$\Delta\epsilon_d$ = radial strain range at the minimum section during each cycle
$\Delta\bar{\epsilon}_d$ = the average radial strain range during the whole life
ϵ_d^0 = the radial strain in the first cycle of loading
ϵ_f = the corresponding radial strain at fracture caused by monotonic (static) loading
$\tilde{\epsilon}$ = a measure of relative static damage ($=\epsilon_d^0/\epsilon_f$)
N_f = the number of cycles to failure
N_{cr} = the number of cycles to crack initiation
C, α = fatigue ductility coefficient and exponent
σ_m = mean stress
σ_e = equivalent stress
d_0 = the initial diameter of the minimum section
d = the current diameter of the minimum section
R = the initial radius of curvature of the notch
D = the initial gross diameter of the round bar
γ = correlation coefficient
m = triaxiality sensitivity parameter

INTRODUCTION

Plasticity in materials is known to play a leading role within the range of low cycle fatigue ($N_f = 10^2$–10^4). Following the J-integral concept of Rice [1], Lamba [2] and Dowling and Begley [3] as applied to cyclic loading conditions, the cyclic J-integral concept, ΔJ can be established. However, strictly speaking, the ΔJ-integral is not path-independent when either the path route is near to the crack tip or owing to other local effects existing in the region ahead of a growing crack

Table 1(a). Chemical composition (%wt) of carbon steels and 20Cr steel

Group	C	Mn	Si	P	S	Cr
A	0.18	0.66	0.24	0.15	0.025	0.01
B	0.20	0.39	0.06	0.01	0.021	0.06
C	0.21	—	0.30	—	—	0.99

Table 1(b). Heat treatments and mechanical properties

Group	Heat treatment	Ultimate strength (MPa)	Yield stress (MPa)
A	Quenched from 880°C and tempered at 710°C for 5 h	444	323
B	Quenched from 895°C and air cooling	506	230
C	Quenched from 880°C and air cooling	605	347

as discussed by Chan *et al.* [4]. So far one of the most successful and widely accepted models, which correlates the amplitude of cyclic plastic strain with fatigue life, is the formulation given by Tavernelli and Coffin [5] and Manson [6]; i.e.

$$\Delta\epsilon_p = CN_f^{\alpha}. \tag{1}$$

Here, $\Delta\epsilon_p$ is a constant plastic strain range enforced on specimens, N_f denotes the number of cycles to failure, C and α are material constants. This formula reflects the importance of plasticity, particularly when the strains are in excess of yielding conditions. This is in contrast with stress cycling, where material strength is a dominant factor.

However, to date, little is known about the fatigue fracture behaviour of materials under large strain cycling whose number of cycles to failure is within the range 1–100. In most cases, such as in the crack-tip or notch-tip zone, strain is accompanied with high triaxiality. Therefore, different shapes of notched bars are needed for testing. Our study shows that this range has a gradual transition feature from static fracture with ductile dimples to cleavage under fatigue conditions. Fractography observation demonstrates a mixed form of microstructural pattern in the intermediate range. Eventually, for the range of $N_f = 1$–100, we propose a modified Coffin–Manson relation associated with a generalized cyclic strain range parameter.

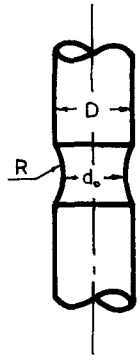

Fig. 1. Specimen shape.

Table 2. Geometrical parameters of the specimens

Material group	Geometrical type	Number of specimens	R (mm)	D (mm)	d_0 (mm)
A	A_1	12	62.0		
	A_2	7	4.5	16.0	9.5
	A_3	9	1.5		
B	B_1	6	40.0	10.0	6.0
	B_2	9	1.5	9.5	
C	C_1	9	40.0	10.0	6.0
	C_2	9	1.5	9.5	

SPECIMENS AND EXPERIMENTAL METHODS

Three types of materials are used for specimens. Both group A and group B are specimens made of carbon steel but with some differences in chemical compositions and heat treatments. Group C uses a 20Cr steel. The details are listed in Table 1(a) and (b).

Various shapes of axisymmetric bars are designed to obtain different triaxiality conditions in the central zone of the specimens. As shown in Fig. 1 and Table 2, each group of specimens is further subdivided into sub-groups, such as A_1 or A_2 etc., to specify the differences in geometrical dimensions.

Group A specimens were tested on a 25-ton MTS-810 testing machine but a Shimadzu (EA 10-EHF) fatigue machine was used for groups B and C. All the tests were carried out at room temperature.

The axial displacement range between the two ends of the MTS machine was controlled for group A, using a triangular displacement waveform ($R = -1$) at the basic frequency of 0.2 Hz. In this case, the amplitude of the diametral deformation at the minimum section varies as load cycling proceeds. The varying diametral deformations were measured by a diametral extensometer provided by the MTS system but adapted by changing one of the flat edges into a knife. For groups B and C, a special extensometer was designed in order to control the radial strains at the minimum section of each bar. The device is a copy of the sketch shown by D'Haeyer and Simon [7]. Its precision is calibrated within the strain range control limits of our tests. In each case, the corresponding hysteresis loops were recorded on an X–Y recorder.

The results of these tests carried out by two research groups, using various materials subjected to different heat treatments and also either varying or keeping approximately constant radial strain range, provide us with a solid ground and a wide scope of conditions to assist our final conclusions.

EXPERIMENTAL OBSERVATIONS

Figure 2(a) and (b) displays some typical hysteresis loops recorded during load cycling, in which, the x-axis denotes (a) the axial displacement range ΔL [Fig. 2(a), group A] and (b) the diametral deformation range Δd [Fig. 2(b), group A]. The y-axis represents load P. Figure 2(a) and (b) belongs to the records of the same specimen taken from group A. Figure 3 is the record of a radial-strain control test in group B, in which the x-axis is the radial strain range $\Delta\epsilon_d$. The curves in Fig. 2(a) and (b) clearly show that, although the axial displacement range ΔL is controlled, the diametral deformation changes with a monotonic trend after each loading cycle. The tension and

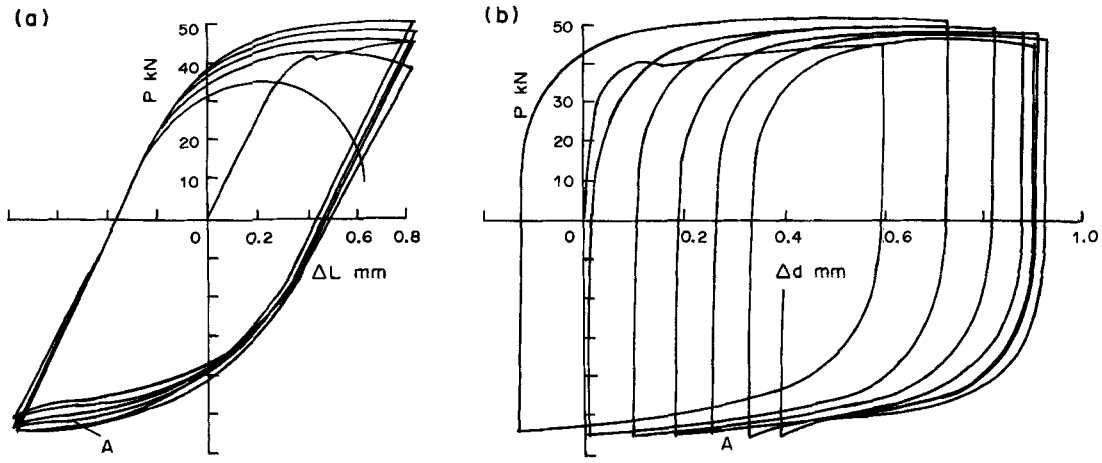

Fig. 2. Hysteresis loops with elongation range controlled. (a) P vs ΔL ($N_f = 8$) and (b) P vs Δd ($N_f = 8$).

compression displacements are symmetric, yet bring about a steady increase in the diameter at the neck of a specimen. Besides the material in group C, the other tests show a cyclic hardening behaviour. Inverted curvature can be seen near the bottom ends of the compression portions of the hysteresis loops when crack closure comes into effect. Once this phenomenon occurs, as specified by "A" in Fig. 2, the earliest fatigue crack can always be seen on the surface of the notch root. The corresponding number of cycles N_{cr} is then called the fatigue life for crack initiation. If the earliest inversion in curvature cannot be distinguished in hysteresis loops, the value of N_{cr} can also be defined as the number of cycles to cause a drop of 5% of load range ΔP from the stabilized values. Crack initiation consumes the major portion of life. The average ratios of N_{cr}/N_f are 0.86 (for A_1), 0.68 (for A_2), 0.56 (for A_3), 0.83 (for B_1), 0.77 (for B_2), 0.87 (for C_1) and 0.79 (for C_2). A smoother notch root results in a larger portion of N_{cr}.

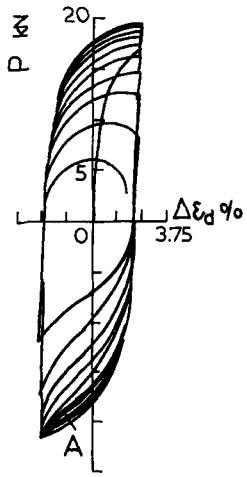

Fig. 3. Hysteresis loops with radial strain range controlled. P vs $\Delta\epsilon_d$ ($N_f = 26$).

Owing to the non-linear behaviour and the non-uniform distributions of the strains around notch roots, we prefer to use the radial strain at the smallest section of the specimens as a parameter for measurement, that is,

$$\epsilon_d = \ln(d/d_0) \tag{2}$$

where, d_0 and d denote the initial and current diameter at the minimum section, respectively. The corresponding radial strain range of each cycle is

$$\Delta\epsilon_d = \epsilon_{d(max)} - \epsilon_{d(min)}. \tag{3}$$

It has been shown that $\Delta\epsilon_d$ varies during cyclic loading of specimens in group A, although the amplitude of axial displacement is controlled. Hence, employing the concept of strain damage accumulation [8], we define $\Delta\bar{\epsilon}_d$ as an average radial strain range, to estimate the damage caused by cyclic straining. So that,

$$\Delta\bar{\epsilon}_d = \frac{1}{N_f}\int_1^{N_f} \Delta\epsilon_d \, dN = \frac{1}{N_f}\sum_{i=1}^{N_f} (\Delta\epsilon_d)_i \quad \text{for group A.} \tag{4}$$

Here $(\Delta\epsilon_d)_i$ denotes the radial strain range of the ith cycle. Naturally, when the radial strain range is controlled approximately to be a constant, then we have

$$\Delta\bar{\epsilon}_d = \Delta\epsilon_d \quad \text{for groups B and C.} \tag{5}$$

In terms of the Coffin–Manson formula, relationships between N_f and $\Delta\bar{\epsilon}_d$ are obtained from tests on each sub-group of specimens. As stated above, $\Delta\bar{\epsilon}_d$ is the average range value of the radial strains accumulated:

$$\begin{aligned}
&\Delta\bar{\epsilon}_d = 0.419 N_f^{-0.590} \quad \gamma = -0.978 \quad \text{for } A_1\\
&\Delta\bar{\epsilon}_d = 0.253 N_f^{-0.510} \quad \gamma = -0.990 \quad \text{for } A_2\\
&\Delta\bar{\epsilon}_d = 0.252 N_f^{-0.593} \quad \gamma = -0.994 \quad \text{for } A_3\\
&\Delta\bar{\epsilon}_d = 0.369 N_f^{-0.504} \quad \gamma = -0.962 \quad \text{for } B_1\\
&\Delta\bar{\epsilon}_d = 0.186 N_f^{-0.522} \quad \gamma = -0.958 \quad \text{for } B_2\\
&\Delta\bar{\epsilon}_d = 0.490 N_f^{-0.555} \quad \gamma = -0.939 \quad \text{for } C_1\\
&\Delta\bar{\epsilon}_d = 0.130 N_f^{-0.500} \quad \gamma = -0.925 \quad \text{for } C_2.
\end{aligned} \tag{6}$$

Here, γ is the correlation coefficient. Each of the equations in equations (6) is a statistical result, taking into account all the data of each sub-group of specimens and using the least square method.

Plotted in Fig. 4(a) in log–log coordinates, are the regression lines based on each sub-group data which display the relation between the number of cycles to failure N_f and the average radial strain range $\Delta\bar{\epsilon}_d$. Three solid lines represent the result of A_1, A_2 and A_3. Broken lines denote those of B_1 and B_2 and dash–dot lines are for C_1 and C_2. Two important factors can be immediately obtained from this figure. That is to say, the material constants C and α of the Coffin–Manson formula in equation (1) correspond to the position and slope of each regression line. However, the lines in Fig. 4(a) are wide-spread. The question then becomes: is there any unified relation with regard to these scattered data?

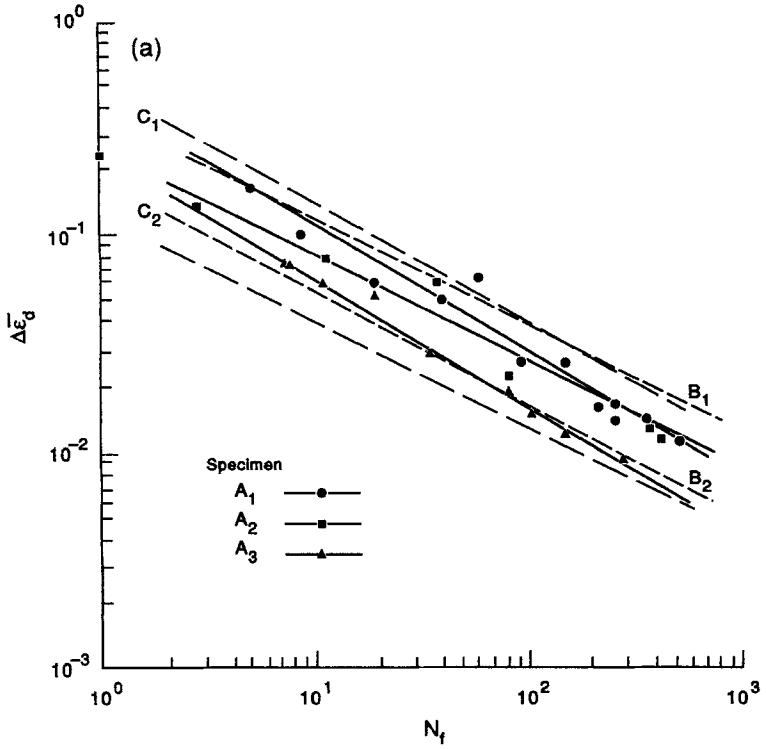

Fig. 4(a). *(Caption opposite).*

A GENERALIZED CYCLIC-STRAIN RANGE

A brief review of recent progress in the understanding of fatigue damage is necessary before we can take any measure to improve the scatter situation. Chell [8] proposed a crack growth damage accumulation model, in which damage is categorized to compose of two parts: one is attributed to the portion caused by static loading, while the other part is due to the fatigue damage accumulated under cyclic loading. Shimada and Furuya [9] developed a model based on a local crack-tip strain concept. Both fatigue crack initiation and propagation were treated under the same material failure condition, when the accumulation of load cyclic strains reached a critical value, this being a function of the number of cycles to failure. Based on these models, we can say that the first part of damage is of a "static" nature which represents the state of a material loaded monotonically to the maximum point (P_{max}) during the first cycle to straining. This static damage must be controlled by the fracture toughness of a material. The second part, called cyclic damage, is a cyclic accumulation of all the reversals of loading. It is assumed to follow the Coffin–Manson relation.

Taking into account both the static and cyclic features of damage, we first define a damage criterion in the form of

$$\frac{\epsilon_d^0}{\epsilon_f} + \frac{\Delta\bar{\epsilon}_d}{CN_f^\alpha} = 1. \tag{7}$$

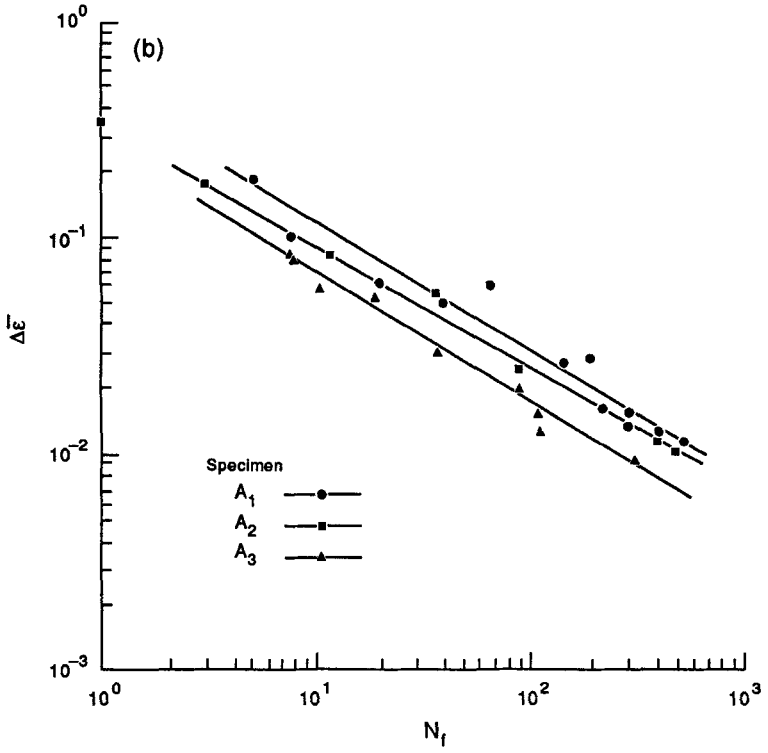

Fig. 4(b)

Fig. 4. The number of cycles to failure N_f as a function of (a) the average radial strain range $\Delta\bar{\epsilon}_d$ ($\Delta\bar{\epsilon}_d$ vs N_f) and (b) the average plastic strain range $\Delta\bar{\epsilon}$ ($\Delta\bar{\epsilon}$ vs N_f).

Here, the first term on the left-hand side refers to the static damage characterized by a parameter $\tilde{\epsilon}$, or say

$$\tilde{\epsilon} = \frac{\epsilon_d^0}{\epsilon_f}. \tag{8}$$

This is the ratio of the loaded strain ϵ_d^0 to the fracture strain ϵ_f, both are along the radial direction. Each specific sub-group, listed in Table 2, has its own value for fracture strain ϵ_f, determined by a static uniaxial test in a standard manner. The second term is an average radial strain range $\Delta\bar{\epsilon}_d$ of the whole life and it is governed by the Coffin–Manson relation.

If we further define an average plastic strain range of the whole lifetime as

$$\Delta\bar{\epsilon} = \frac{\Delta\bar{\epsilon}_d}{1-\tilde{\epsilon}} \tag{9}$$

then equation (7) takes a modified form of the Coffin–Manson formula as

$$\Delta\bar{\epsilon} = CN_f^{\alpha}. \tag{10}$$

As the number of cycles to failure moves from $N_f = 10^2$ and eventually reduces to $N_f = 1$, the proportion of static damage characterized by $\tilde{\epsilon}$ is in a status that can be taken, respectively, as negligible ($\leqslant 0.02$), small ($\leqslant 0.08$) and substantial (>0.10). Table 3 clearly shows this trend.

Equation (7) satisfies two extreme cases. When $\tilde{\epsilon} \to 0$, it reduces to the original Coffin–Manson relation. However, if $\tilde{\epsilon}$ becomes so dominant that $\Delta\bar{\epsilon}_d \to 0$, then it refers to the pure static fracture criterion, $\epsilon_d^0 = \epsilon_f$.

For the sake of simplicity and clearness, we may just use the samples from group A to exemplify our approach to unify the experimental data.

Let us first handle the data from group A by using the average plastic strain range $\Delta\bar{\epsilon}$ as a generalized cyclic strain. Instead of the three equations leading in equations (6), we now have

$$\begin{aligned} \Delta\bar{\epsilon} &= 0.468 N_f^{-0.609} \quad \gamma = -0.979 \quad \text{for } A_1 \\ \Delta\bar{\epsilon} &= 0.359 N_f^{-0.576} \quad \gamma = -0.994 \quad \text{for } A_2 \\ \Delta\bar{\epsilon} &= 0.304 N_f^{-0.625} \quad \gamma = -0.994 \quad \text{for } A_3. \end{aligned} \tag{11}$$

This step makes the maximum difference between the values of α change from $-0.510 + 0.593 = 0.083$ to $-0.576 + 0.625 = 0.049$ with better conditions for the correlation coefficient γ. As shown in Fig. 4(b), although the three regression lines are still separate, they are now more or less parallel with each other.

Additional efforts are then made to bring together the three almost parallel lines. The aim is achieved by taking into account the influence of the triaxiality conditions in the central zone of each type of specimen. The parameter σ_m/σ_e, which is the ratio of mean stress to equivalent stress, is adopted to characterize the actual degree of the triaxial stress state. According to the close form of the formula given by Bridgman [10] for calculating the stresses in axisymmetric bars, we find

$$\frac{\sigma_m}{\sigma_e} = \frac{1}{3} + \ln\left(\frac{d_0}{4R} + 1\right) \tag{12}$$

Table 3. $\tilde{\epsilon}$ versus N_f in specimens of group A

A_1		A_2		A_3	
$\epsilon_f = -0.695$		$\epsilon_f = -0.530$		$\epsilon_f = -0.442$	
N_f	$\tilde{\epsilon}$	N_f	$\tilde{\epsilon}$	N_f	$\tilde{\epsilon}$
509	0.0106	431	0.0117	283	0.0099
381	0.0124	360	0.0158	152	0.0158
273	0.0129	84	0.0245	104	0.0212
265	0.0141	37	0.0566	82	0.0245
217	0.0140	12	0.0753	37	0.0387
144	0.0150	3	0.2217	20	0.0758
93	0.0181	1†	0.3768	11	0.0772
64	0.0210			8	0.1456
41	0.0261			8	0.1240
20	0.0351				
9	0.0561				
5	0.1171				

in which, the geometrical notations follow the specifications in Fig. 1, d_0 and R denote, respectively, the minimum diameter of the specimen and its notch radius before loading. The results for the three sub-groups A_1, A_2 and A_3 are listed in the bottom line in Table 4. However, in the case of a large strain condition, the curvature of the local notch changes depending on both its initial profile and the stage of straining. As strain increases, the sharp notch is blunted and may become smoother (such as in A_3). On the contrary, a smooth notch sharpens after the occurrence of necking (for example, in A_1 and A_2). Employing the large-strain finite-element computational results of Yang and Li [11], we have the results of σ_m/σ_e given in Table 4, which take into account the large strain effects stated above. They are related to the number of cycles to failure, since N_f depends on the amplitude of strain. Although the value of σ_m/σ_e varies along the radial direction of the bar, in our tests, we take the maximum value related to the centre as the nominal representative for each subgroup.

To include the triaxiality effect of stress, we further modify the strain range parameter $\Delta\bar{\epsilon}$ given in equation (9) by defining a generalized cyclic strain range $\Delta\epsilon$ as

$$\Delta\epsilon = \frac{1}{1-\tilde{\epsilon}} \left[\frac{\frac{\sigma_m}{\sigma_e}}{\left(\frac{\sigma_m}{\sigma_e}\right)_0} \right]^m \Delta\bar{\epsilon}_d \tag{13}$$

Here, $(\sigma_m/\sigma_e)_0$ is a value based on the standard smoothly notched bar used for fatigue tests. At the initial moment of loading, it has the value of $(\sigma_m/\sigma_e)_0 = 0.37$. The term m is an experimental parameter depending on the material used; it reflects the sensitivity of materials to the notch condition. In fact, the sequence displayed by the three lines in Fig. 4(b) is in accordance with the degree of triaxiality existing in each sub-group of specimens.

The whole factor $((\sigma_m/\sigma_e)/(\sigma_m/\sigma_e)_0)^m$ plays the role of bringing the three almost parallel lines in Fig. 4(b) together into one solid line of group A, as is shown in Fig. 5.

The determination of the parameter m is based on a statistical process, by using the experimental data of each group of samples. With regard to the value chosen for m and its corresponding correlation coefficient γ, a relation curve can be drawn for each group of specimens. The value of

Table 4. The corresponding values of σ_m/σ_e with respect to N_f

	A_1		A_2		A_3	
	N_f	σ_m/σ_e	N_f	σ_m/σ_e	N_f	σ_m/σ_e
	509	0.42	431	0.81	283	1.18
	381	0.43	360	0.81	152	1.18
	273	0.43	84	0.85	104	1.18
	265	0.43	37	0.88	82	1.18
Yang and Li [11]	217	0.43	12	0.88	37	1.18
	144	0.43	3	0.89	20	1.20
	93	0.44	1	0.89	11	1.15
	64	0.44			8	1.11
	41	0.44			8	1.14
	20	0.44				
	9	0.45				
	5	0.45				
Bridgman [10]	—	0.37	—	0.76	—	1.28

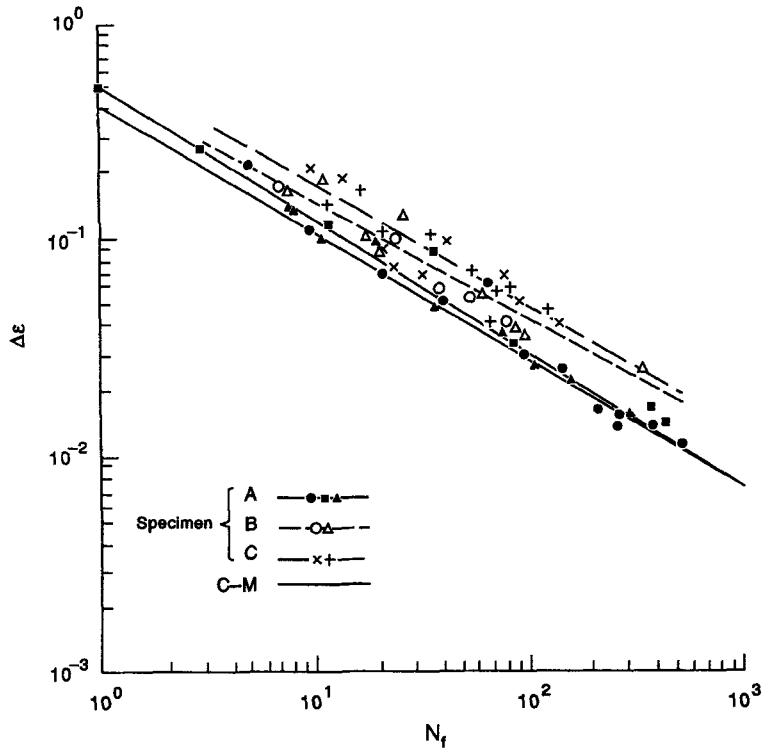

Fig. 5. The number of cycles to failure N_f as a function of the generalized cyclic strain range $\Delta\epsilon$ ($\Delta\epsilon$ vs N_f).

m which can yield a relative maximum γ is taken as the actual parameter and shown in Table 5. Materials of better ductility have a lower value of m, and are less sensitive to the triaxiality effect.

We may now assume that the new generalized cyclic strain range $\Delta\epsilon$ in equation (13), follows the Coffin–Manson relation, so that

$$\Delta\epsilon = CN_f^{\alpha}. \tag{14}$$

In the case of small-strain low-cycle fatigue, $\tilde{\epsilon} \to 0$ and $(\sigma_m/\sigma_e) \to (\sigma_m/\sigma_e)_0$, then equation (14) reduces to equation (1), or say

$$\Delta\epsilon(\text{or } \Delta\bar{\epsilon}_d) = \Delta\epsilon_p = CN_f^{\alpha} \tag{15}$$

Table 5. The parameters used in equation, (13) and (14) with $(\sigma_m/\sigma_e)_0 = 0.37$

Group	m	C	α	γ
A	0.45	0.515	−0.609	−0.986
B	0.88	0.521	−0.543	−0.960
C	1.34	0.683	−0.567	−0.929

in which, $\Delta\bar{\epsilon}$ denotes an average plastic strain to substitute the constant strain range, when the amplitude of strain varies during the life time. All the regression lines in Fig. 4(a) are given in this sense, although most of the samples have undergone large straining, the effects of static damage and life reduction caused by triaxiality are not yet taken into account.

Figure 5 shows the regression lines obtained from equations (13) and (14) for groups A, B and C. Each line has a very satisfactory condition in terms of the correlation coefficient. This situation indicates that we can indeed unify the experimental data of each material to one regression line by taking into account the static damage and triaxiality effect. A thin line is depicted in Fig. 5 and is marked as C–M for the result of the original Coffin–Manson relation, using the data of group A only. This line is obviously the lowest line, along with the heavily modified line. Both regression lines tend to coincide, only when N_f approaches to 10^3, because then the effects of static damage and stress triaxiality become negligible. But, our modification provides a better fitting line for the experimental data within the range of $N_f = 1$–100.

This fact supports and proves the validity of modifying the original Coffin–Manson relation by substituting a generalized cyclic strain $\Delta\epsilon$. More confidence is felt, since the results are mutually checked by the two sets and test arrangements stated previously. One set is the material in group A subjected to varying amplitudes of strains. Another is conducted with the materials of groups B and C, using rather constant cyclic strain range at the minimum diameter of each specimen.

Although our modification given in equation (13) might look as empirical as the Coffin–Manson relation does, our efforts should not be taken as an arbitrary manipulation of curve fitting. Actually, the original notion for the formulation or derivation of equation (13) can only be obtained through a thorough understanding of the mechanical nature existing in the range concerned and searching for the influential factors which have previously been neglected. The revelation of these factors is further shown by the following study on the material fracture mechanisms.

SEM AND TEM OBSERVATIONS

The fracture mechanism of materials subjected to high triaxial stress and large strain cycling, undergoes a transition from ductile tearing to fatigue cleavage. It depends on the number of cycles to failure N_f or equivalently on the extent of the generalized cyclic strain range $\Delta\epsilon$. After rupture, the fracture surfaces of the group A specimens were examined by a scanning electron microscope (SEM). Some typical pictures are selected and shown in Fig. 6. Figure 6(a) is the fracture surface of a specimen with $N_f = 431$. It has a typical nature of low-cycle fatigue. There is a fatigue source near the zone marked by the letter "a". Then stream lines specified by A, B, C etc. emanate from this source and are located between cleavage areas. Tiny voids can be seen spreading in and near these curve lines. A similar feature is also seen in other samples with a relatively high value of N_f. But no obvious fatigue source nor stream lines are found among the group A specimens when N_f is lower than 100.

Figure 6(b) displays the picture from a specimen with $N_f = 93$. It is clear that fatigue cleavage is still a dominating mechanism of fracture. However, voids are now seen widely dispersed and dotted on the cleavage surface in a random manner instead of being localized within some of the stream lines as in Fig. 6(a).

In striking contrast to the previous two pictures, Fig. 6(c) provides an enhanced nature of ductile fracture when the number of cycles to failure reduces to $N_f = 37$. Here, voids and dimples are found to be gathering together within an area. Microcracks are also developed.

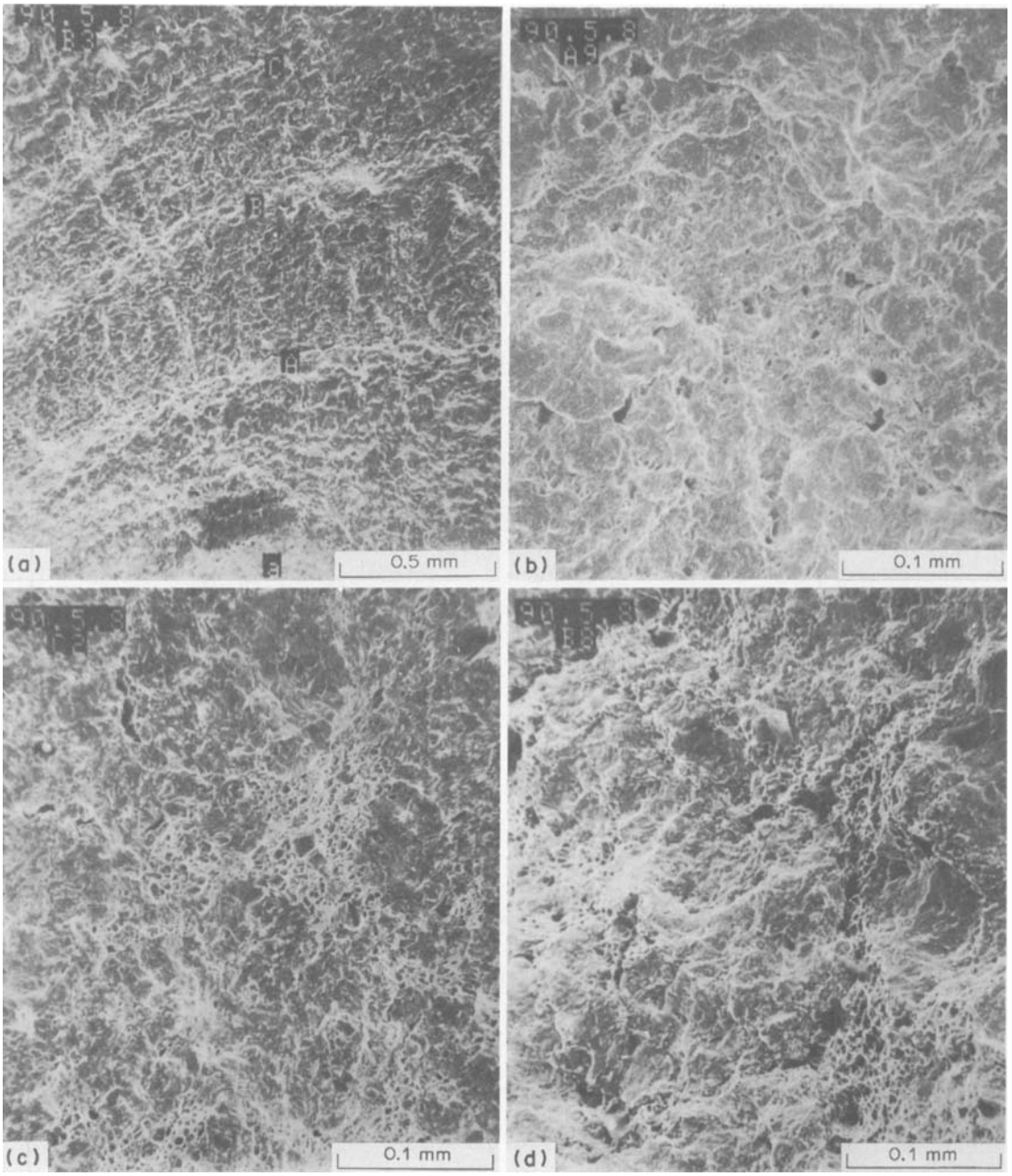

Fig. 6. Scanning electron micrographs.

Lastly, the fracture surface ruptured by cyclic loading for $N_f = 12$ is shown in Fig. 6(d). Scattering large voids and tearing regions together with microcracks are seen. The whole surface has a fibrous and uneven nature.

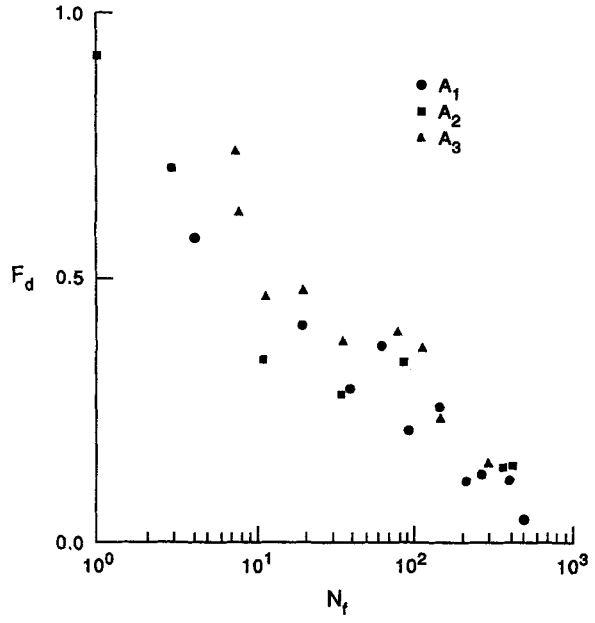

Fig. 7. Dimpled area fraction F_d vs cycles to failure N_f.

The fractography study stated above is quantified by using an image analysis system to measure the amount of dimpled area within each picture, which is a magnification of an area of $150 \times 180\,\mu$m. Five such areas are randomly chosen to obtain an average evaluation of a ductility parameter, nominated as the dimpled area fraction F_d, which is the proportion of dimpled area within each area of each specimen taken for observation. The data thus obtained from the specimens of group A are shown on Fig. 7, which clearly demonstrates a descending trend of the dimpled area fraction F_d with respect to the number of cycles to failure N_f.

This microstructural study strongly supports the view that static ductile damage does participate in material failure with a monotonically increasing degree, as N_f decreases (or $\Delta\epsilon$ increases). The effect is associated with the triaxiality condition which affects the initiation and growth of voids.

The steels used for groups B and C are high stacking-fault-energy materials. Dislocations patterned as cell wall structures are usually found in such steels under cyclic loading. According to the report of Feltner and Laird [12], the cell size increases as the plastic strain amplitude decreases. Their observations were made after the specimens were cyclically strained at two different amplitudes for 20 and 1000 cycles. These numbers of cycles corresponded to 20% of the life of the specimens. Therefore, the situation in the cases of N_f less than 100 should be investigated.

Thin film samples were made from the specimens of groups B and C for a transmission electron microscope (TEM) study. Figure 8 presents dislocation cell wall structures located in two specimens subjected to different amplitude cyclic strains which eventually cause the material to fail at $N_f = 32$ and 142. A few tangled dislocations are still seen within each cell. Statistical analysis, based on the known method of linear intercept, provides us with the data given in Fig. 9 for the cell size parameter $\bar{d}$. We extended the observation to the cases with N_f less than 100. Again, the cell size

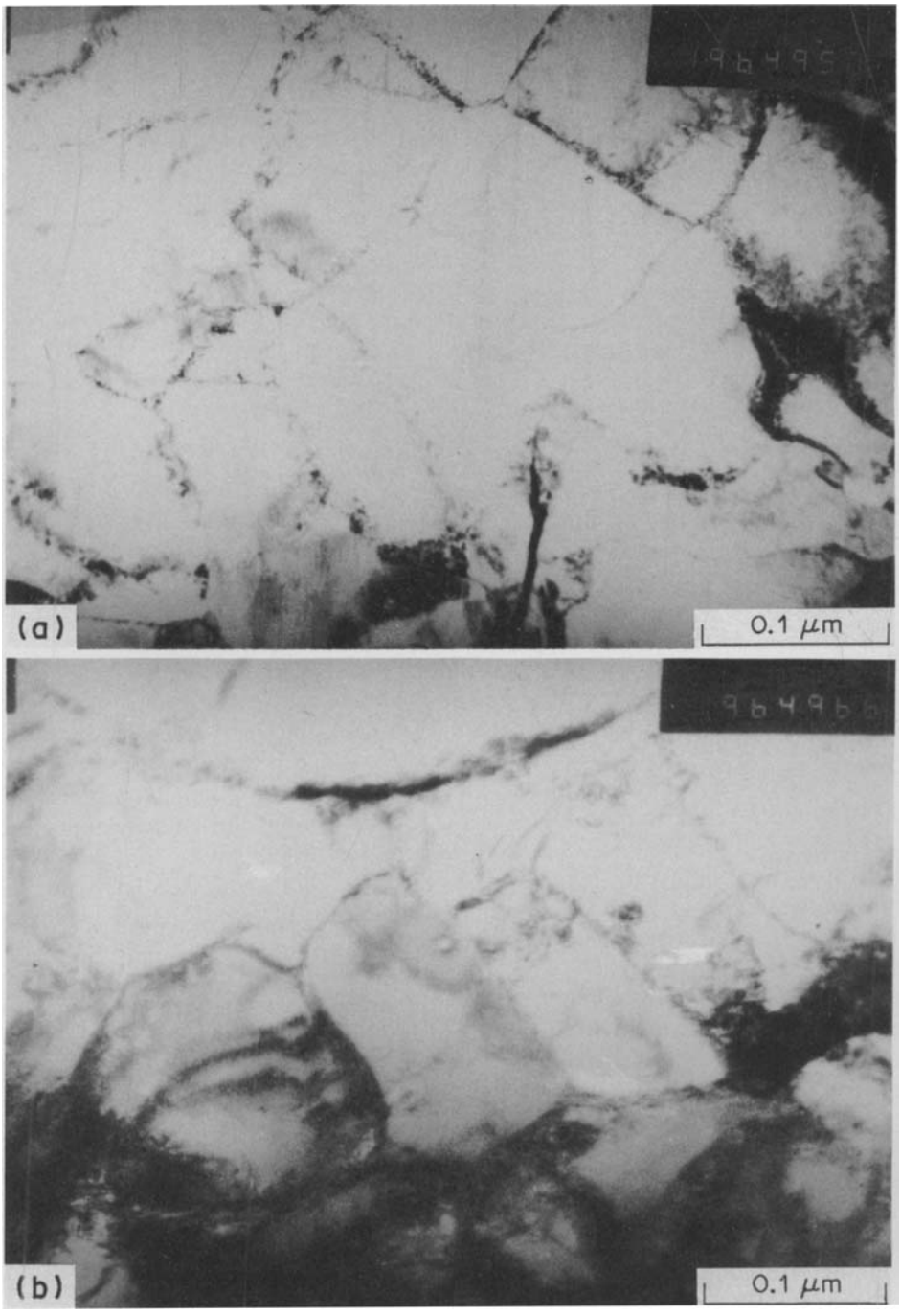

Fig. 8. A comparison of dislocation cells. (a) $N_f = 32$ and (b) $N_f = 142$.

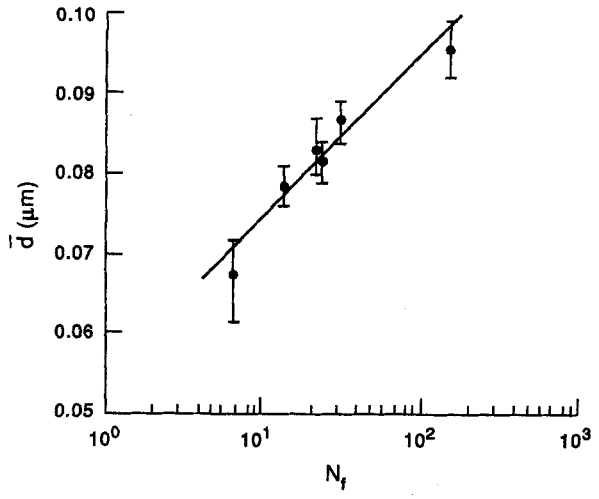

Fig. 9. Dislocation cell size $\bar{d}$ versus cycles to failure N_f.

$\bar{d}$ is seen to be decreasing with the decrease of the number of cycles to failure, or the increase of the amplitude of cyclic strains.

CONCLUSIONS

(1) A definition of generalized strain range $\Delta\epsilon$ is provided as a characterizing parameter to describe the fracture behaviour of materials subjected to high triaxial stress and large strain cyclic loading. This modification extends the applicability of the Coffin–Manson formula to the range of cycles to failure N_f, i.e. 10^0–10^2 cycles. The parameter $\Delta\epsilon$ includes the following factors:

(a) the average plastic strain range $\Delta\bar{\epsilon}_d$ enforced during cyclic loading,
(b) the effect caused by static damage $\tilde{\epsilon}$,
(c) the high triaxial tension stress influence reflected by the factor $[(\sigma_m/\sigma_e)/(\sigma_m/\sigma_e)_0]^m$.

(2) The ratio value of N_{cr}/N_f, is dependent on the triaxiality condition. It decreases as the local radius of a notch root decreases, or the triaxiality increases.

(3) Fractography studies demonstrate that the microstructure at failure undergoes a transition from ductile dimple to fatigue cleavage, when the cycles to failure N_f varies from 10^0 to 10^3.

(4) Microscopic observations also prove that dislocation cell size increases as the amount of the generalized strain range $\Delta\epsilon$ decreases or the corresponding cycles to failure N_f increases from 10^0 to 10^2.

Acknowledgement—Financial support offered by the Chinese Academy of Sciences is gratefully appreciated.

REFERENCES

1. J. R. Rice (1968) A path independent integral and the approximate analysis of strain concentration by notches and cracks. *Trans. Am. Soc. Mech. Engrs, J. Appl. Mech.* **35**, 379–386.
2. H. S. Lamba (1975) The J-integral applied to cyclic loading. *Engng Fract. Mech.* **7**, 693–703.

3. N. E. Dowling and J. A. Begley (1976) Fatigue crack growth during plasticity and the J-integral. ASTM STP 590, pp. 82–103.
4. K. S. Chan, J. Lankford and D. L. Davidson (1986) A comparison of crack-tip field parameters for large and small fatigue cracks. *Trans. Am. Soc. Mech. Engrs, J. Engng Mater. Technol.* **108,** 206–213.
5. J. F. Tavernelli and L. F. Coffin Jr (1962) Experimental support for generalized equation predicting low cycle fatigue. *Trans. Am. Soc. Mech. Engrs, J. Basic Engng* **84,** 533–537.
6. S. S. Manson (1962) Discussion. *Trans. Am. Soc. Mech. Engrs, J. Basic Engng* **84,** 537–541.
7. R. D'Haeyer and P. Simon (1982) Low cycle fatigue behaviour of thick high-strength steel plates for pressure vessels. ASTM STP 770, pp. 296–310.
8. G. G. Chell (1984) Fatigue crack growth laws for brittle and ductile materials including the effects of static modes and elastic–plastic deformation. *Fatigue Engng Mater. Struct.* **7,** 237–250.
9. H. Shimada and Y. Furuya (1987) Local crack-tip strain concept for fatigue crack initiation and propagation. *Trans. Am. Soc. Mech. Engrs, J. Engng Mater. Technol.* **109,** 101–106.
10. P. W. Bridgman (1952) *Studies in Large Flow and Fracture*, pp. 9–37. McGraw–Hill, New York.
11. G. Y. Yang and G. C. Li (1986) Computer simulation of the ductile fracture behaviour in axisymmetric bars. In *Computer Modelling of Fabrication Processes and Constitutive Behaviour of Metals* (Edited by J. J. M. Too), pp. 385–396. Ottawa, Canada.
12. C. E. Feltner and C. Laird (1967) Cyclic stress–strain response of F.C.C. metals and alloys—II. Dislocation structures and mechanism. *Acta metall.* **15,** 1633–1653.